JOURNAL OF CATALYSIS 132, 128–144 (1991)

Vanadia Catalysts on Anatase, Rutile, and TiO_2(B) for the Ammoxidation of Toluene: An ESR and High-Resolution Electron Microscopy Characterization

MEHRI SANATI,* L. REINE WALLENBERG,† ARNE ANDERSSON,* SUSAN JANSEN,‡ AND YANPING TU‡

*Department of Chemical Technology and †Department of Inorganic Chemistry 2, Chemical Center, Lund Institute of Technology, P.O. Box 124, S-221 00 Lund, Sweden; and ‡Department of Chemistry, Temple University, Philadelphia, Pennsylvania 19122

Received January 28, 1991; revised May 9, 1991

Three titania polymorphs, anatase, rutile, and TiO_2(B), were used as supports for vanadia. Catalysts with nominal loadings corresponding to 1.5 and 5 theoretical layers were prepared. True monolayer samples were obtained by NH_3(aq)-treatment of the samples with 5 nominal vanadia layers. Prepared catalysts were characterized by chemical analysis, ESR, and high-resolution electron microscopy. It was observed that an almost complete monolayer of vanadia can be formed on anatase and TiO_2(B). The monolayer on TiO_2(B) consists of V^{4+} species. A magnetic species attributable to tetrahedral states of vanadium was found to dominate the ESR resonance. Chemical analysis of the monolayer on anatase showed the presence of both V^{4+} and V^{5+} species. The ESR spectrum indicated a high degree of V^{4+}–V^{4+} interaction. From the characterizations of rutile-supported samples it seems that the support interface is a solid solution of V^{4+}. On all supports, vanadium on top of the monolayer is present as V^{5+}. High-resolution micrographs of the samples with the highest loading revealed the formation of amorphous vanadia on both anatase and rutile. On TiO_2(B), vanadia was found to grow coherently at the titania interface. The catalysts were used in the oxidation and ammoxidation of toluene to benzaldehyde and benzonitrile, respectively. Considering both activity and selectivity, multilayers of vanadia supported on TiO_2(B) show a good performance for both reactions.

INTRODUCTION

Titania-supported vanadium oxide catalysts are active and selective for the partial oxidation and the ammoxidation of alkylaromatic compounds (*1–6*). The catalytic properties of the active phase can be expected to be influenced by the choice of titania polymorph used as support. In several cases, anatase rather than rutile has been reported to be preferred (*7–9*). Véjux and Courtine (*10*) have demonstrated the existence of a crystallographic fit between the (010) plane of V_2O_5 and the (001) and (010) faces of anatase. Thus, a preferential exposure of V_2O_5 (010) should be expected on anatase. Investigation of anatase samples with low vanadia loading using X-ray absorption spectroscopy (*11*), however, showed the existence of disordered vanadia species bonded to the titania surface via two bridging oxygen species. Additionally, there are two oxo-groups at each vanadia species. Also, several other investigators have concluded that anatase modifies the properties of vanadia by the formation of a stable monolayer of vanadia species directly bonded to the surface of the support (*2, 9, 12*). On rutile, on the other hand, the vanadia/titania interaction is weak (*13*) leading to formation of crystalline V_2O_5 under reaction conditions (*9*). However, Trifirò and coworkers (*14*) have not found the crystalline structure of TiO_2 to be crucial for the amount of vanadia strongly interacting with the support. Rather, the most important factor is the degree of surface hydroxylation, which greatly depends on the method of

0021-9517/91 $3.00

preparation. Characterization of mono- and multilayers of vanadia on TiO_2 suggests a chemical and catalytic difference between the two regions (*3, 15–17*).

Recently, we have found the TiO_2(B) polymorph (*18*) of titania suitable as support for vanadium oxide, when used in the ammoxidation of toluene to benzonitrile (*6*). The structure and catalytic property of the active phase were found to depend strongly on the vanadia loading. In the present investigation we report a characterization and comparison of anatase, rutile, and TiO_2(B) as supports for vanadia. The catalysts were characterized by IR, ESR, high-resolution electron microscopy (HREM), and chemical analysis, and they were used in the (amm)oxidation of toluene.

EXPERIMENTAL

Preparation of Supports

Preparation of TiO_2(B). The support precursor was prepared by mixing KNO_3 with TiO_2(anatase) in a mole ratio $KNO_3 : TiO_2$ of 1.2 : 2. The mixture was calcined at 950°C for 44 h. According to X-ray diffraction, the major part of the product was $K_2Ti_4O_9$, JCPDS 27–447 (*19*). Then the precursor was hydrolyzed for 3 days at room temperature using a 0.45 *M* nitric acid solution. For each mmole of precursor, 100 ml of the acid solution was added. After filtration and drying at 40°C for 24 h, the product was calcined in a flow of air for 3 h at 450°C. X-ray diffraction analysis showed that the final product was pure TiO_2(B), JCPDS 35–88 (*19*). The mechanism of formation of TiO_2(B) from $K_2Ti_4O_9$ has recently been clarified (*20*).

Preparation of rutile. A solution of titanium(IV) was prepared by dissolving pure $TiCl_4$ in an aqueous solution of hydrochloric acid with pH $\approx$ 0. $TiCl_4$ was added slowly at room temperature while stirring. At the same temperature precipitation was performed by the slow addition of NH_3(aq) while stirring. The resulting precipitate was filtered off and washed with water until free of chloride ions. The product was dried overnight at 80°C and then calcined in a flow of O_2 at 800°C for 6 h. According to X-ray diffraction, the product was almost pure rutile, JCPDS 18–1404 (*19*). The anatase content was 3%, as determined using the equation given by Spurr and Myers (*21*).

Anatase support. The anatase sample used in this study was a commercial sample (Merck 99%). According to X-ray diffraction, JCPDS 21–1272 (*19*), it was pure anatase.

TABLE 1

Loading and Surface Area of Catalysts

Catalyst[a]	Loading[b] (mg V_2O_5/m^2)	S_B[c] (m^2/g)	S_A[d] (m^2/g)
VT_A-6	6.03	9.6	5.2
VT_B-6	6.06	13.7	11.4
VT_R-6	6.05	6.0	4.3
VT_A-1.9	1.86	9.6	8.3
VT_B-1.9	1.87	18.3	11.0
VT_R-1.9	1.87	6.0	5.7
VTM_A	0.84	9.6	7.7
VTM_B	1.20	13.7	10.9
VTM_R	1.20	6.0	4.6

[a] VT_A, VT_B, VT_R were obtained by wet impregnation of anatase, TiO_2(B), and rutile polymorphs, respectively. The VTM samples were obtained by NH_3(aq)-treatment of the corresponding VT-6 samples.

[b] Expressed per surface area of fresh support.

[c] Surface area per gram of support before impregnation.

[d] Surface area per gram of catalyst after impregnation.

Preparation of Catalysts

Anatase, TiO_2(B), and rutile were used as supports for vanadium oxide. Two methods of catalyst preparation were used in this study. The first method was standard wet impregnation of the support with solutions of varying concentrations of ammonium metavanadate. Six samples with different loadings were prepared. Their loadings, also included in the catalyst notation, and specific surface areas are given in Table 1. From the unit cell dimension of V_2O_5 (*22*), an average value for a loading corresponding to a complete monolayer can be calculated as

1.2 mg V_2O_5/m^2 surface area of support, if the (100), (010), and (001) planes are considered. Considering Table 1, it can be concluded that the loadings on each support correspond to 1.5 and 5 theoretical layers.

In the second preparation method, samples originally having a loading of five theoretical layers were treated with conc. NH_3(aq). After drying, the samples were calcined in air at 450°C for 3 h. Titrimetric analysis showed that, depending on the titania polymorph, different amounts of vanadium remained after NH_3(aq)-treatment. The remaining vanadium content and specific surface area of these samples are included in Table 1.

After sieving, the fractions of particles with diameters in the range 0.150–0.425 mm were used in the experiments.

Characterization of Catalysts

X-ray diffraction analysis of the catalysts was carried out on a Philips X-ray diffraction instrument using a PW 1732/10 generator and Cu$K\alpha$ radiation.

The specific surface areas of the samples were determined with a gravimetric BET apparatus using adsorption of N_2 at liquid N_2 temperature.

Chemical analysis of the amount of vanadium on the catalysts was performed using a procedure similar to that described in the literature (*3*, *14*). First the catalyst sample was treated with a 25 wt% aqueous solution of NH_3 at room temperature for 15 h. The solid part was filtered off and the pH of the solution adjusted to 1 with H_2SO_4. The solid part was further treated with hot 4 *M* H_2SO_4. The two solutions thus obtained were analyzed for their total content of vanadium and its degree of reduction. For this purpose titrations were made with standardized solutions of $KMnO_4$ and $(NH_4)_2Fe(SO_4)_2 \cdot 6H_2O$ (*23*). In the latter case, a few drops of diphenylamine dissolved in H_3PO_4 was used as an indicator.

FTIR spectra were recorded using a Mattson Polaris spectrometer equipped with a Harrick Scientific Praying Mantis diffuse reflection attachment. Before recording of ν(OH) bands, the undiluted samples were evacuated at 300°C for 4 h. For this purpose a reaction chamber of stainless steel from Harrick Scientific Corp. was used. It was provided with KBr windows, which were mounted in a stainless-steel dome. The sampling cup was at the top of a stainless-steel rod in which both the heating cartridge and the thermocouple were embedded. The temperature was controlled with a Love 301 self-tune controller. The body of the chamber was cooled by circulating water. The pressure was measured with two MKS vacuum gauges. A resolution of 4 cm^{-1} was used, and 1000 spectra were collected for each sample. ICON analytical software from Mattson Instruments was used for spectral treatment.

For the study of metal–oxygen IR vibrations, the samples were diluted with 85 wt% of KBr. Spectra were recorded without further treatment in dry air free of CO_2.

ESR experiments were performed with a Bruker ER-200-D system, which was equipped with an ER035 gaussmeter, a field frequency controller and counter, and a VT4104 variable temperature assembly.

High-resolution micrographs were recorded with a JEM 4000EX transmission electron microscope, with an interpretable resolution of 0.16 nm in projected crystal structures. A JEM 2000FX scanning transmission microscope, equipped with a Link AN 10000 energy dispersive spectrometer (EDS), was used for preliminary investigations and elemental analysis.

Simulated diffraction patterns and sphere structure models were produced for all major zone axes in rutile and anatase with a multipurpose computer program suite (*24*). These were compared to recorded selected area diffraction patterns and HREM images. Because of the small size and agglomeration of the particles, the zone axis orientations of the HREM images were further verified by optical diffraction in an optical bench with a laser light source.

When investigating surface features on the atomic level it is of vital importance to avoid contamination. To ensure clean sur-

faces, all samples were kept in microscope vacuum (3×10^{-5} Pa) for at least 12 h before final examination. Apart from the quality of the vacuum, the growth rate of amorphous contamination in the microscope is strongly dependent on both the nature of the sample and the current density of the electron beam. A low-dose technique was used for primary photographic recordings. An image-intensified TV camera was used for correction of astigmatism and of focus at low-beam current density and magnification (usually 150–500 kx). Thereafter the electron beam could be concentrated and the growth of contamination could be followed on the TV monitor. The growth rate could be as high as 3 nm/min in a fully converged beam (20–40 Å/cm^2), but was found to be negligible at the low current density used for recording of the low-dose images.

The catalytic performance of prepared catalysts was studied for the oxidation and ammoxidation of toluene to benzaldehyde and benzonitrile. Carbon oxides were formed as the main by-products. A differential and isothermal plug flow reactor held at 370°C was used in the experiments. Over 0.1–0.3 g of catalyst, diluted with quartz of the same particle size, a total flow of 186 standard cm^3/min was passed. The partial pressures of toluene and oxygen were 0.77 and 11.4 kPa, respectively, while the partial pressure of NH_3 was varied from 0 to 5.71 kPa. Nitrogen was used as an inert gas. Reaction products were analyzed on a Varian Vista 6000 gas chromatograph. Reactor and analysis arrangement were the same as described elsewhere (*25*).

RESULTS

Chemical Analysis

The results of analysis of the catalysts with respect to vanadium content and the average oxidation number of vanadium using titrimetric methods are given in Table 2. Two types of vanadium were found, one soluble and the other insoluble in NH_3(aq). The latter part was analyzed after dissolution in conc. H_2SO_4. In the case of anatase and TiO_2(B)-supported catalysts, addition of the amounts of the two types of vanadium gave a value in agreement with the total loading, which was determined by atomic absorption analysis after complete dissolution of catalysts in conc. HF. For rutile samples, however, the vanadium content determined by titrimetric methods was found to be less than the amount originally deposited. This can be due to formation of a solid solution of vanadium in rutile. Consideration of the amount of vanadium, which is insoluble in NH_3(aq), especially for anatase and TiO_2(B) samples, shows that this amount is close to the theoretical monolayer capacity. This observation indicates the possibility that the vanadia insoluble in NH_3(aq) constitutes a monolayer interacting with the titania interface. A comparison of the average oxidation numbers of vanadium interacting with the different titania polymorphs shows striking differences. On TiO_2(B) and rutile supports, the oxidation state of the interacting vanadium is +4, while on anatase the average oxidation number is +4.8. At high loadings, there are additional layers on top of the monolayer. For all supports, the oxidation number of vanadium in the multilayer region is +5. The data given in Table 2 are representative for catalysts both freshly pre-

TABLE 2

Chemical Analysis of Catalysts

Catalyst	Soluble in NH_3(aq)		Insoluble in NH_3 (aq)		
	V/V_{tot}	ON[a]	V/V_{tot}	% of mono	ON[a]
VT_A-6	0.86	5.0	0.14	70	4.8
VT_B-6	0.80	5.0	0.20	100	4.0
VT_R-6	0.80	5.0	0.15	75	4.0
VT_A-1.9	0.50	5.0	0.50	75	4.8
VT_B-1.9	0.48	5.0	0.52	78	4.0
VT_R-1.9	0.16	5.0	0.26	39	4.0
VTM_A	0	—	1.00	70	4.8
VTM_B	0	—	1.00	100	4.0
VTM_R	0	—	0.29	29	4.0

[a] ON, average oxidation number of vanadium.

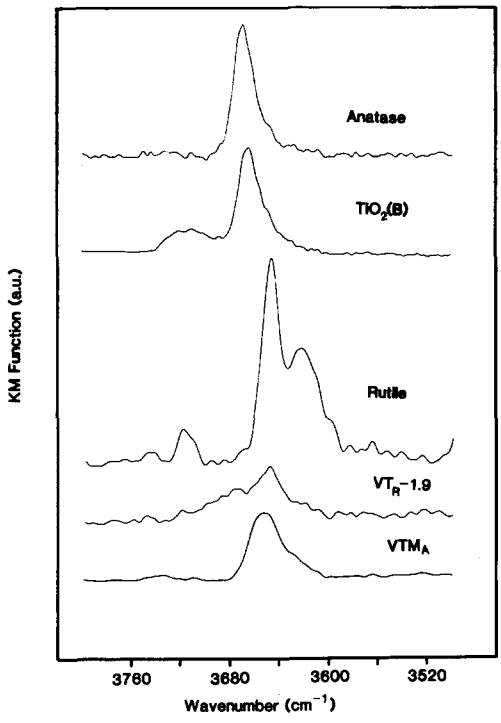

FIG. 1. Diffuse reflectance FTIR spectra of ν(OH). The spectra are normalized with respect to surface area.

pared and after being used for several hours in ammoxidation experiments, where the partial pressure of NH_3 was varied from low to high values.

Infrared Spectroscopy

Evacuation at 300°C for 4 h caused a substantial decrease in the intensity of water deformation bands. The OH stretching region after evacuation is shown in Fig. 1. Pure anatase has a relatively intense band at 3670 cm^{-1} and a shoulder can be distinguished at 3651 cm^{-1}. A sharp ν(OH) band for pure TiO_2(B) centers at 3666 cm^{-1} and a weak broadband is at about 3720 cm^{-1}. Pure rutile shows bands at 3622, 3647, and 3720 cm^{-1}. Also a shoulder is seen at 3599 cm^{-1}. After evacuation of the supported catalysts, only VT_R-1.9 and VTM_A show bands in the OH stretching region. The VT_R-1.9 sample shows a weak Ti–OH band from rutile at 3647 cm^{-1}. A band at 3652 cm^{-1} and a shoulder at 3627 cm^{-1} are observed for VTM_A. These bands are possibly V–OH bands of monolayer species (*26, 27*).

In order to illustrate the level of vanadium content at which crystalline V_2O_5 starts to form, the overtone region of the fundamental V=O stretching vibrations is shown in Fig. 2. In the infrared spectra of supported catalysts, V_2O_5 bands at 2020 and 1974 cm^{-1} (*6, 28, 29*) are observed only at high loadings, i.e., in case of VT_A-6, VT_B-6, and VT_R-6. These bands are the first overtones of the fundamentals appearing at 1020 and 985 cm^{-1} (*30*). Figure 2 implies that formation of crystalline V_2O_5 is more favored on anatase support.

ESR Spectroscopy

Figure 3 shows the ESR spectra recorded at 100 K for the catalysts with the lowest vanadium loadings. The corresponding spectra for the samples with the highest loading showed a single line spectrum similar to V_2O_5. Room-temperature spectra for the anatase and rutile samples provided lim-

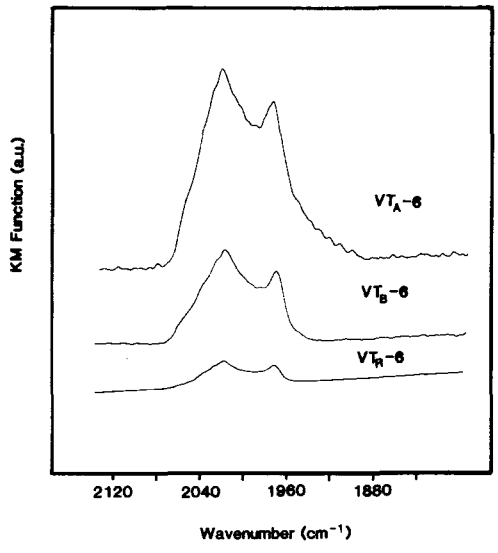

FIG. 2. FTIR spectra of the overtone region of fundamental vanadyl stretching vibrations. The spectra are normalized with respect to surface area.

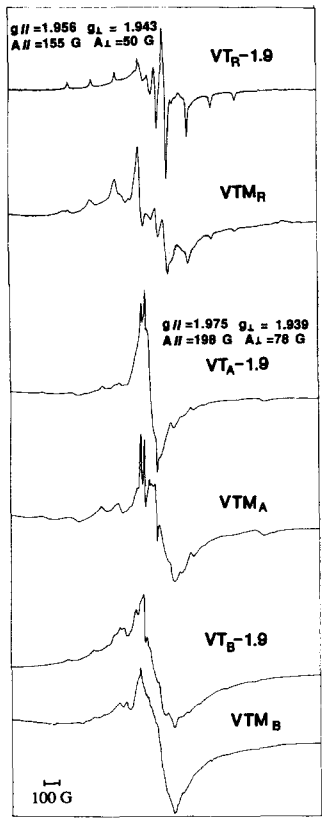

FIG. 3. ESR spectra of some catalysts.

ited resolution. For the TiO_2(B) samples, well-resolved hyperfine features could be observed at room temperature for VT_B-1.9 while the VTM_B showed a broad resonance, thus demonstrating different limits in dipolar exchange.

Electron Microscopy

Anatase support. The support particles were approximately in the size range 50–150 nm and usually agglomerated. Pure anatase proved to be more stable in the electron beam compared to vanadia-coated samples. Apart from this, the particles appeared very similar before and after vanadia deposition.

Using the low electron dose technique, images of the pure support surfaces without any appreciable amorphous overlayer or surface structures could be obtained. Figure 4 shows a section of a spherical particle, which is approximately 64 nm in diameter. The amorphous contamination or radiation product from the support was less than 0.5 nm at any point around the periphery of the particle.

After deposition of an amount of vanadia corresponding to five theoretical V_2O_5 layers, no clean support surfaces could be found. This was the case even when using the low-dose technique on previously unexposed areas. Typically, an amorphous vanadia overlayer approximately 2.5 nm thick was found to cover the support particles. Figure 5 shows the rounded edge between a (1,0, − 1) and a (0,1, − 1) surface. The amorphous layer was of even thickness on both facets as well as the connecting bent surface shown in the figure. This finding is opposed to a previous investigation (*31*), which reported a preferential sticking to certain crystal planes.

The observed instability of the impregnated anatase sample toward the focused electron beam can be partly explained by the particles changing their orientation relative to the beam. By watching the convergent beam diffraction pattern and the Kikuchi lines in reciprocal space, it was observed that vicinal zone axes moved collectively, without change of the interconnecting distance. This implies a pure rotation without any phase change. Since the particles were always almost spherical, the effect of a small change in alignment is very striking and thickness fringes were seen traversing the particles. In some cases they could be realigned by using the tilt mechanism of the microscope. Apart from the local heating effect, the rotation is also facilitated by the vanadium oxide layer at the interfaces between particles, since it is known that vanadium oxide is quite easily reduced *in situ* by the electron beam (*32, 33*). Previously, this has been attributed to the formation of a superstructure, or possibly a rutile-like solid solution (*34*).

Rutile support. The rutile particles were

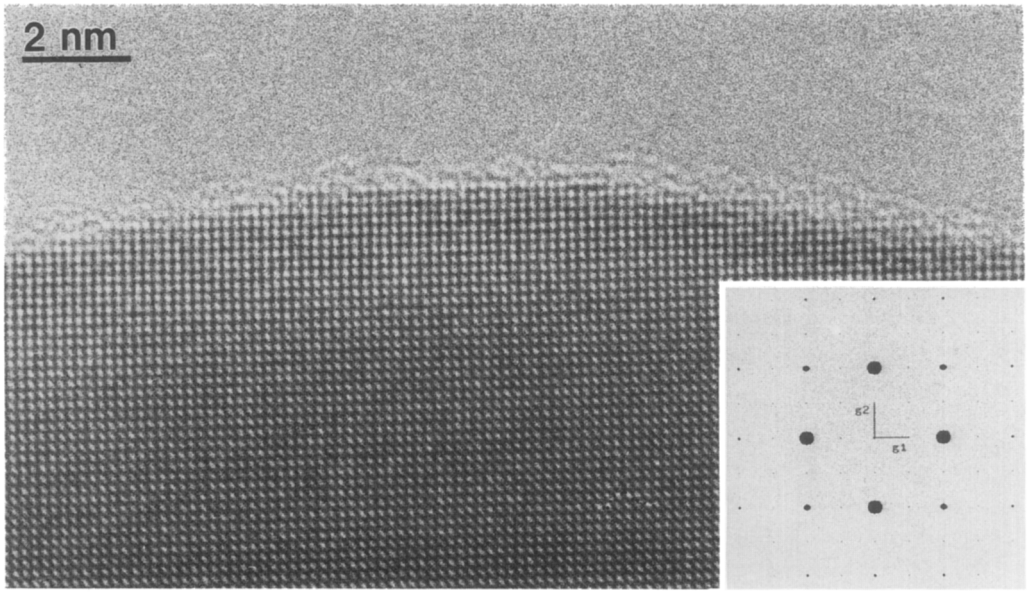

FIG. 4. Low-dose high-resolution image of the anatase support before deposition of vanadium oxide. The viewing direction is [001] and the distance between the orthogonal (200) and (020) fringes is 0.189 nm. The surfaces appear clean and the amorphous contamination layer is less than 0.5 nm.

generally more poorly crystallized, slightly smaller, and more irregular in size than the anatase support particles. In this case, even the pure support was quite unstable in the beam. On some occasions, however, clean surfaces could be imaged using the low-dose technique. The surfaces generally appeared rougher than in the case of anatase, which made it more difficult to establish the thickness of the amorphous surface layer when present on the impregnated support.

In the case of the VT_R-6 catalyst, it was clearly observed that the amount of amorphous material was significantly less than that for VT_A-6. Figure 6 shows a reasonably sharply facetted rutile particle imaged in surface profile mode. Single-atom steps are visible on the otherwise flat surface. The zone axis orientation was verified through optical, simulated, and recorded diffraction patterns. Using the identified spacings for accurate scaling of the image, the thickness of the amorphous layer was determined to be less than 1.5 nm, as compared to 2.5 nm for VT_A-6. Thus it seems that some of the vanadium has formed a solid solution in the rutile.

The vanadium at the surface can be reduced *in situ* by the electron beam, which earlier has been shown to be the case for TiO_2(B)-supported samples (*33*). In the latter case VO_x, $0.8 \leq x \leq 1.2$, a metal oxide with a basic defected sodium chloride structure was formed (*35*). Figure 7 shows an image of a spherical VT_R-6 particle where a few VO_x-particles have been formed by beam irradiation of an otherwise clean surface.

TiO_2(B) support. Results from electron microscopy investigations of support and TiO_2(B)-supported catalysts (*33, 36*) have been presented elsewhere, and will only be discussed briefly here.

The support particles are rod-like with a typical width and length of around 0.2×8 μm. In contrast to anatase and rutile supports, the TiO_2(B) particles are quite stable in the electron beam even when vanadium oxide has been deposited.

It has been suggested (*33, 36*) that the

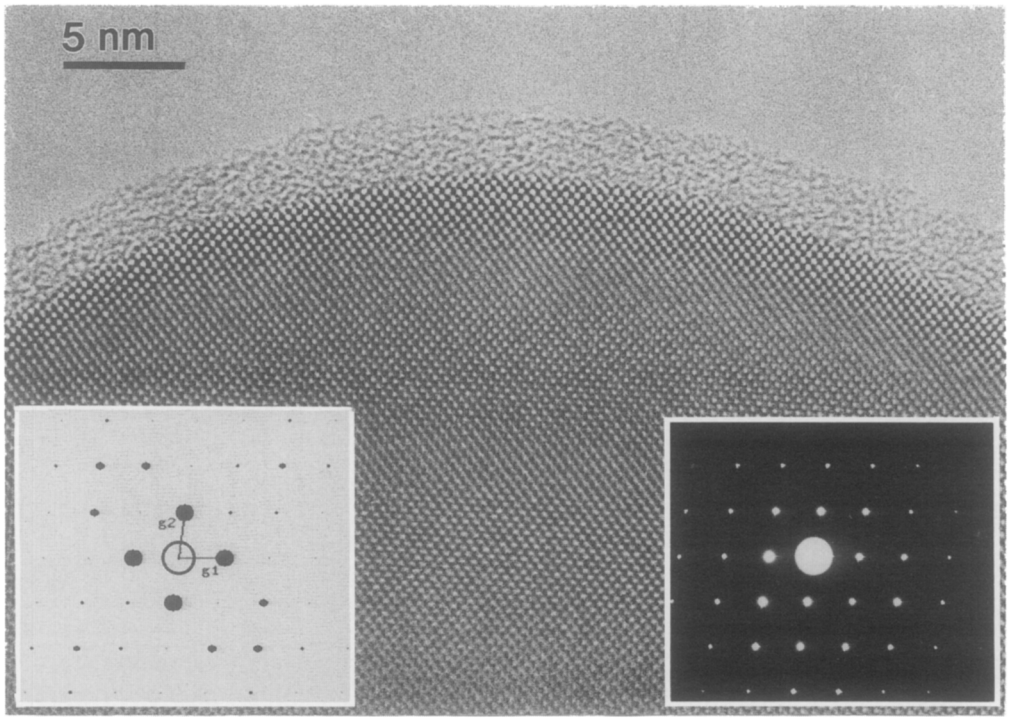

FIG. 5. Typical low-dose image of the anatase support with a loading corresponding to five theoretical V_2O_5 layers (VT_A-6). The titania surface is covered with an amorphous vanadia layer, which is approximately 2.5 nm thick. The electron beam is parallel to [111]. The left inset shows a simulated electron diffraction pattern ($g_1 = (1,0,-1)$; $g_2 = (0,1,-1)$). The right inset shows the recorded selected area diffraction pattern. 110- and 202-type of reflections are present due to dynamical diffraction.

first layer formed on the support surface is epitaxially grown VO_2(B) (*37*), which is isostructural with TiO_2(B) (*18*). This model was concluded from the absence of visible surface structures in HREM images of catalysts with low loadings, possibly due to identical structures and the similar scattering power of Ti and V. Apart from FTIR measurements and EDS mapping, the presence of vanadium on the surface was also proven by irradiation with a focused electron beam. Irradiation produces reduced vanadium oxide particles on the surfaces, which is shown in Fig. 8. The apparent epitaxy of the VO_x-particle in Fig. 8b is purely coincidental. Normally, no epitaxial relationship with the support is observed.

Formation of V_2O_5. At high vanadia loadings, several indications were obtained for formation of some crystalline V_2O_5, especially, on the surface of anatase and TiO_2(B)-supported catalysts, e.g., by the use of X-ray powder diffraction and FTIR analyses.

Small V_2O_5 particles could be identified on VT_B-6 through their lattice spacing and ability to be reduced in the beam. Figure 9a shows a particle with the main spacing consistent with d_{200} in V_2O_5 (0.576 nm) (*22*), according to optical diffraction. After a few minutes in the beam, the crystal became reduced to VO_x (Fig. 9b). The beam direction was [110] and the (002)- and (111)-type spots were identified in the optical diffractogram.

Performance of Catalysts in the (Amm)oxidation of Toluene

In Figs. 10–12, the rate per unit surface area for the formation of benzonitrile over the prepared catalysts is plotted as a func-

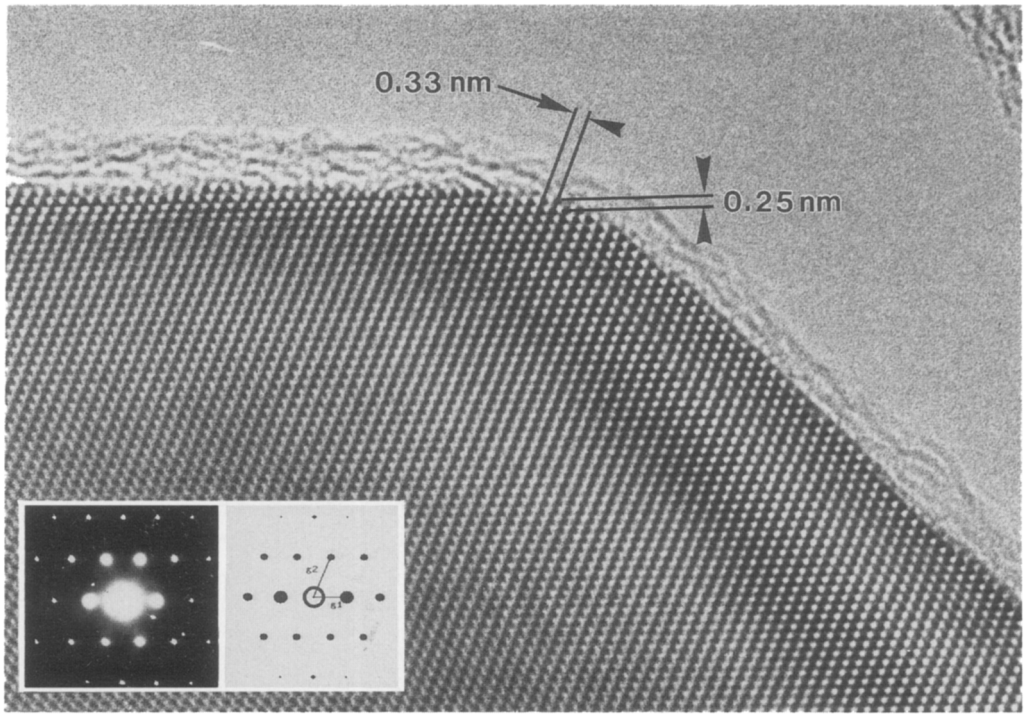

FIG. 6. A crystal of the VT_R-6 catalyst viewed along the [111] direction. The indicated spacings of 0.33 and 0.25 nm are between (−1,0,1) and (−1,1,0) atom planes, respectively, corresponding to the g_1 and g_2 vectors in the inset recorded and simulated diffraction patterns. The amorphous layer is less than 1.5 nm and markedly thinner than the corresponding layer on the VT_A-6 catalyst, which indicates a solid solution of vanadium in rutile.

tion of the partial pressure of NH_3. For all catalysts, the rate passes through a maximum at low pressure of NH_3 and at high pressures the rate declines slowly with increase in pressure.

At a vanadium loading of five theoretical layers, Fig. 10, the rutile- and TiO_2(B)-supported catalysts are more active than the anatase-supported catalyst. Also, all supported catalysts are more active than unsupported crystalline V_2O_5. A comparison of the selectivity values for the formation of benzonitrile, which are included in Fig. 10, shows that the highest selectivity was obtained over the TiO_2(B)-supported catalyst.

The rate and selectivity for nitrile formation over VT_B-1.9 and VT_A-1.9 (Fig. 11) are comparable to those measured over VT_B-6 and VT_A-6 (Fig. 10). However, the rate over VT_R-1.9 is only half of that for VT_R-6. Data for VTM_A, VTM_B, and VTM_R catalysts with a loading in the monolayer range are given in Fig. 12. It is seen that the performances of VTM_B and VTM_A are almost identical and that they give rates for nitrile formation higher than those with VTM_R and all other preparations.

Rates and selectivities for the formation of benzaldehyde measured in the absence of NH_3 are given in Table 3. There is a general tendency toward an increase in both rate and selectivity with increase in vanadium loading, with the exception that VT_R-6 is slightly less selective than VT_R-1.9. The activity and selectivity for aldehyde formation over the monolayer samples VTM_A, VTM_B, and VTM_R are less than the values for crystalline V_2O_5. Only total combustion was observed over VTM_B. The VT_A-1.9, VT_B-1.9, and VT_R-1.9 samples have activities that are

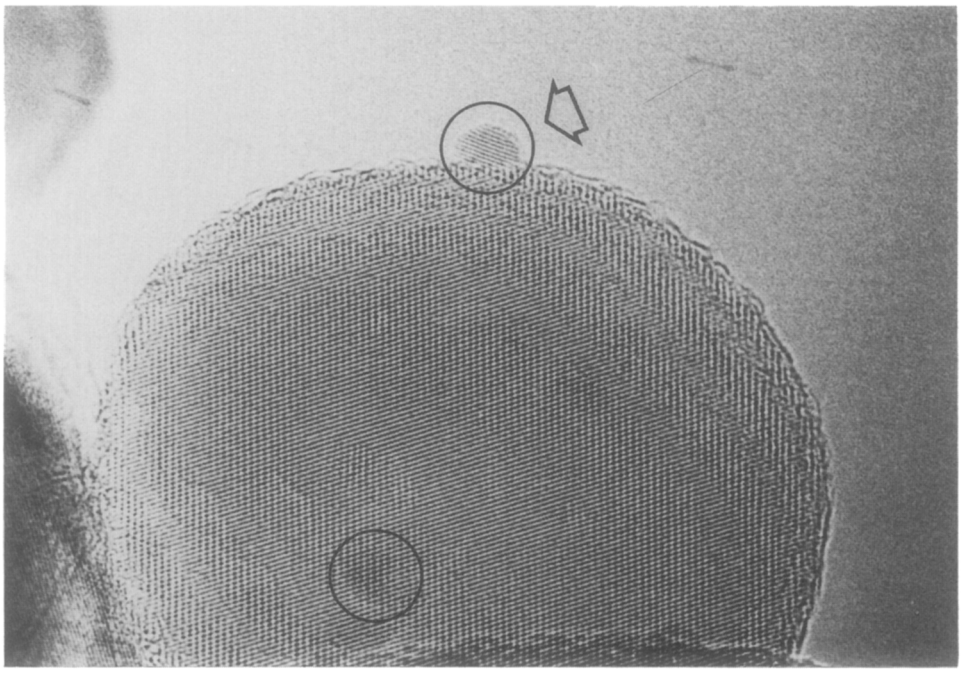

FIG. 7. Occasionally, evidence of particle formation was found. The image shows a spherical crystal (approximately 38 nm in diameter) of impregnated rutile with two encircled particles. According to optical diffraction, the spacing in the arrowed particle is 0.210 ± 0.007 nm, which is possibly the (200) spacing (0.206 nm) in VO_x. VO_x, thus formed by *in situ* reduction of vanadium oxide, has a basic rock salt structure.

comparable to that of crystalline V_2O_5, although some differences in selectivity values can be observed. At the highest loading, VT_R-6 and VT_B-6 are most active; however, VT_A-6 is most selective.

DISCUSSION

Structure of Active Phase

Monolayer region. It has been proposed that vanadium oxide interacting with silica and γ-alumina is insoluble in an ammoniacal solution (*38*). Support that this is also the case for TiO_2-supported vanadia catalysts can be found in the literature (*3, 6, 29, 39*). In the present study, this inference is verified by the fact that for the catalysts with the highest loading (VT_A-6, VT_B-6, VT_R-6), the fraction of vanadia found to be insoluble in NH_3(aq) according to Table 2 constitutes 70, 100, and 75% of a theoretical monolayer on anatase, TiO_2(B), and rutile, respectively. A high dispersion and an interaction between vanadia and titania is also in agreement with the disappearance of Ti–OH infrared bands upon deposition of vanadia (Fig. 1).

TiO_2(B) monolayer. In an earlier investigation of TiO_2(B)-supported catalysts, it was found that the amount of vanadia that is insoluble in NH_3(aq) rapidly increases with increase in loading and at high loadings never exceeds 100% of a theoretical monolayer (*6*). Also, as seen in Table 2, all the deposited vanadium can be dissolved in treatments with NH_3(aq) and conc. H_2SO_4. It should be mentioned that TiO_2(B) is not dissolved in these treatments. These results show that the vanadia species, which are insoluble in NH_3(aq), are at the titania interface and do not form a solid solution in TiO_2(B). HREM imaging of samples with a low coverage (*33, 36*), showed that any

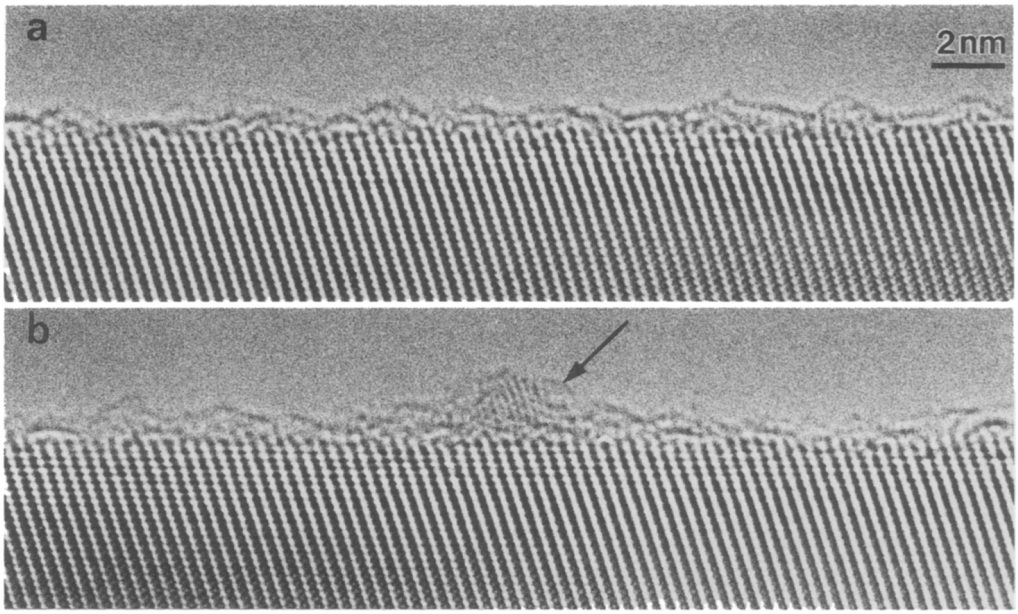

FIG. 8. (a) HREM image of an apparently clean surface of VT_B-6. The unit cell *b*-axis is parallel with the surface. (b) The same crystal after irradiation with the electron beam. A particle (arrowed) of reduced vanadium oxide is formed on the surface.

vanadia phase could only be distinguished after prolonged exposure of the sample to a fully converged electron beam, leading to reduction and formation of VO_x with $0.8 \leq x \leq 1.2$. This observation implies an epitactic growth process upon deposition of vanadia on TiO_2(B). According to the chemical analysis, the vanadia species interacting with TiO_2(B) is in oxidation state +4. Consequently, the monolayer possibly has a VO_2(B)-like structure. In VO_2(B), which is isostructural with TiO_2(B), the vanadium has an octahedral coordination (*37*). The latter coordination is not supported by reported IR spectra (*6*), which indicates the monolayer species to be tetrahedrally coordinated having one oxo-group. This anomaly was explained as being due to atomic scale roughness of TiO_2(B) surfaces (*33*); cf. Fig. 8. At the rough surfaces, possibly formed as a consequence of the acid leaching of the titanate precursor, a substantial amount of vanadium interacting with the support can be expected to be undercoordinated, thus explaining a tetrahedral coordination at low coverage.

The presence of tetrahedral monolayer species on TiO_2(B) is further supported by the ESR spectral envelope in Fig. 3 of VT_B-1.9, which shows features arising from multiple magnetic species. Our recent spectral simulation (*40*) suggested the presence of at least two vanadia species in addition to a third broad feature, which was not simulated. At coverages below three layers of vanadia, a magnetic species, which may be attributable to tetrahedral states of vanadium, was found to dominate the resonance. An absolute analysis of the spin density gave a value of 1.65×10^{-4} mole V^{4+}/g-catalyst for VT_B-1.9. This value agrees well with the number determined by chemical analysis, which is 1.82×10^{-4} mole V^{+4}/g-catalyst. The ESR spectrum in Fig. 3 of the VTM_B sample shows increased dipolar broadening and the resolution of multiple magnetic species cannot be made. Thus, the monolayer produced by NH_3(aq)-washing may be a reg-

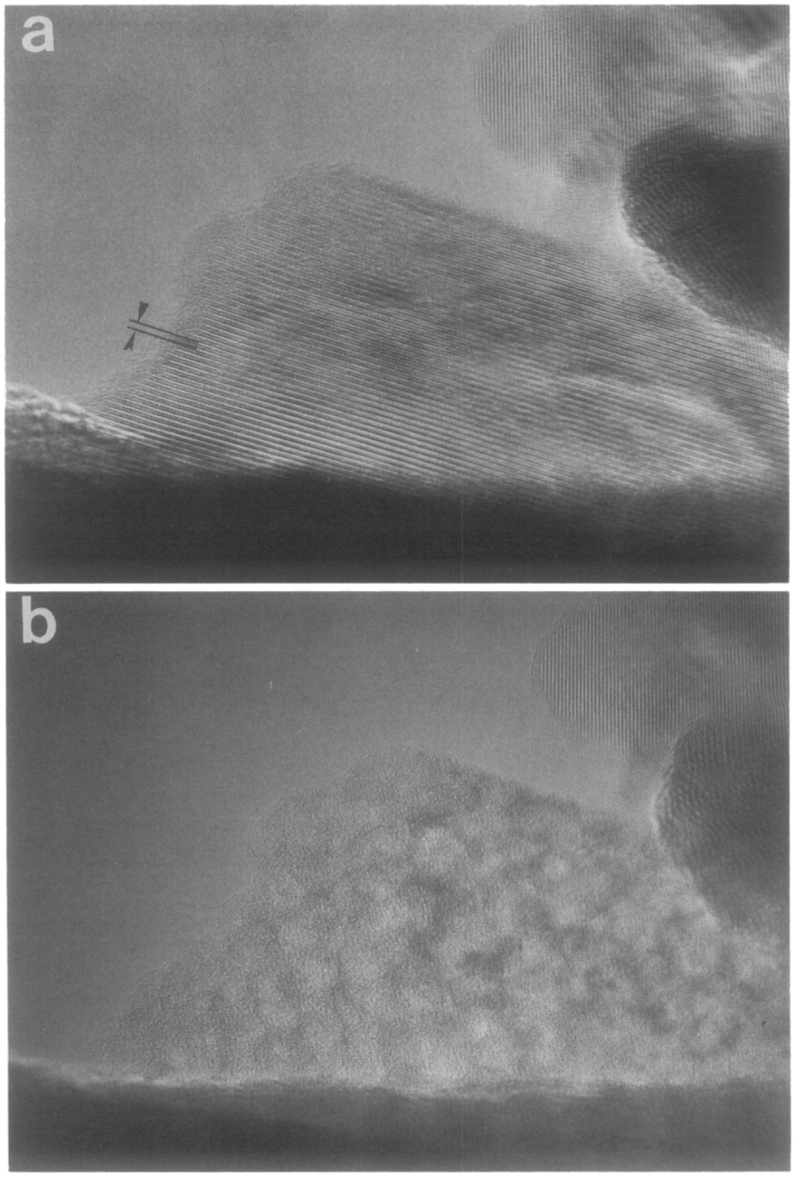

FIG. 9. (a) A particle, approximately 30 nm thick, found on the surface of VT_B-6. The indicated spacing corresponds to d_{200} in V_2O_5. (b) On irradiation, the V_2O_5 quickly transforms to VO_x, which can be identified by the (002) and (111) reflections in the optical diffraction patterns. The corresponding spacings are 0.204 and 0.237 nm, respectively. Note that the surrounding TiO_2(B) support particles are virtually unaffected by the electron beam.

ular layer in which V^{+4}–V^{+4} interactions dominate. Formation of a layer of interconnected vanadia species is in agreement with the result of chemical analysis, which in the case of VTM_B shows the presence of a complete monolayer.

Anatase monolayer. The ability of vanadia to wet anatase surfaces is well known (*9, 13*). In agreement with this ability, the absolute amount of vanadia found to be insoluble in NH_3(aq) is almost the same for VT_A-6 and VT_A-1.9 (Table 2). Considering

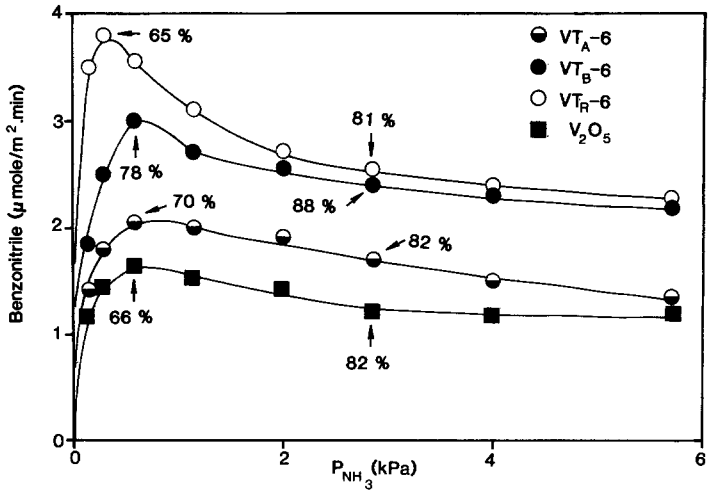

FIG. 10. Rate for formation of benzonitrile over 5-layer catalysts versus partial pressure of NH_3. The partial pressures of toluene and oxygen were 0.77 and 11.4 kPa, respectively. Selectivity values for nitrile formation are inserted.

these values, it can be concluded that the monolayer capacity on anatase is about 70–75% of a theoretical layer. This high value is in agreement with those obtained by others (*15, 41*), even though considerably lower values have also been reported (*5, 17, 29, 42*). According to the chemical analysis, the average oxidation number of monolayer vanadia is 4.8, indicating 80% of V^{5+} species and 20% of V^{4+} species. Also, Trifirò and co-workers have found both V^{4+} and V^{5+} species interacting strongly with anatase (*3*,

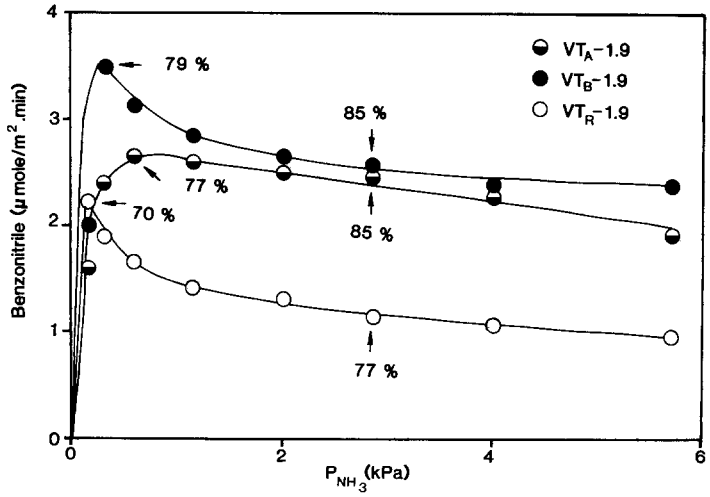

FIG. 11. Rate for formation of benzonitrile over 1.5-layer catalysts versus partial pressure of NH_3. The partial pressures of toluene and oxygen were 0.77 and 11.4 kPa, respectively. Selectivity values for nitrile formation are inserted.

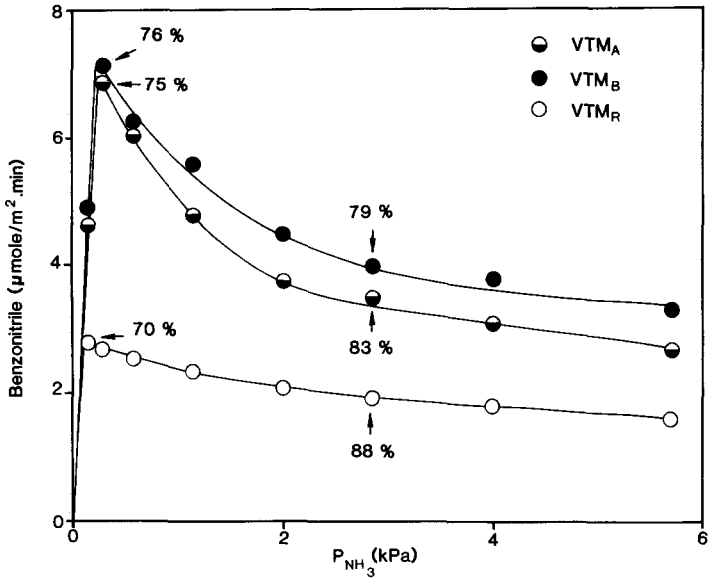

FIG. 12. Rate for formation of benzonitrile over NH_3(aq)-treated catalysts versus partial pressure of NH_3. The partial pressures of toluene and oxygen were 0.77 and 11.4 kPa, respectively. Inserted are selectivities for nitrile formation.

29, 43). However, they proposed (*3*) that the true monolayer was built up from V^{4+} species since with increase in loading, the amount of V^{4+} species approached at constant value close to that of a theoretical monolayer. Other investigators, on the basis of EXAFS (*11*), XPS (*5*), and TPR (*15, 17*) results, have concluded that the monolayer on anatase is fully oxidized. Our result is in close agreement with that of Gasior *et al.* (*8*). They reported about 15% of V^{4+} around monolayer coverage.

The presence of V^{4+} species on anatase was confirmed by ESR (Fig. 3). The primary resonance, in the VT_A-1.9 sample, is a broad line displaying weakly resolved hyperfine components. Similar spectral features are shown by the VTM_A sample; however, a large shift in the $\langle g \rangle$ is observed. This is readily apparent in Fig. 3 as the spectra are aligned with magnetic field position. Simulation of these spectra show a small component of the signal arising from V^{4+} in a "rutile-like" environment. The shift in $\langle g \rangle$ for the VTM_A sample is the result of a greater density of V^{4+}/rutile states. A high degree of V^{4+}–V^{4+} interaction is in both cases suspected because of the poor resolution of hyperfine components.

The infrared spectrum for VTM_A in Fig. 1 shows a band at 3652 cm^{-1} and a shoulder at 3627 cm^{-1}. Clearly, these are not anatase bands. From a comparison with reported spectra (*26, 27*), it can be suggested that they are V–OH bands from monolayer species. Our infrared investigation of anatase and rutile-supported samples did not permit the study of vanadium–oxygen vibrations in the region below 1100 cm^{-1} due to the strong absorption of the support. In our previous study of TiO_2(B)-supported samples, resolution of ν(VO) fundamentals was found possible (*6*). However, Cristiani *et al.* (*44*) using Raman and IR spectroscopy concluded that the monolayer on anatase consists of monoxo-vanadyl species. Therefore, it seems reasonable to assign the monolayer as interconnected oxyhydroxy species in agreement with the proposal of Bond *et al.* (*15*). This assignment, however, is in con-

TABLE 3

Activity and Selectivity for the Formation of Benzaldehyde[a]

Catalyst	Activity (μmole/m^{2}min)	Selectivity (%)
VT_A-6	1.90	56
VT_B-6	3.80	51
VT_R-6	4.10	40
VT_A-1.9	1.64	56
VT_B-1.9	2.00	37
VT_R-1.9	1.70	45
VTM_A	1.00	13
VTM_B	0.00	0
VTM_R	1.22	29
V_2O_5	1.70	45

[a] 370°C. The partial pressures of toluene and oxygen were 0.77 and 11.42 kPa, respectively.

flict with the conclusion based on EXAFS data (*11, 41*) that the monolayer consists of monodispersed VO_4 units with two bridging oxygens and two projecting oxo-species.

Rutile monolayer. It is well known that V^{4+} dissolves in rutile forming a solid solution (*45*). Formation of a solid solution in the case of VT_R-6, VT_R-1.9, and VTM_R can be concluded from the data in Table 2. In the treatments with NH_3(aq) and conc. H_2SO_4, the total amount of vanadium loaded was not dissolved. Thus, the missing part must be in the rutile lattice. For VT_R-6, VT_R-1.9, and VTM_R this amount is 5, 58, and 71%, respectively, of their total content of vanadium, corresponding to 25, 87, and 71%, respectively, expressed in terms of the theoretical monolayer capacity. The indication of a relatively smaller amount of V^{4+} in rutile at the highest loading can be explained by an adhesion of V^{4+} species to superlayer vanadia stronger than that to titania. Support for this conclusion is also found by comparing the values for VT_R-6 and VTM_R. After dissolution of V^{5+} species in NH_3(aq) and further calcination, the absolute amount of V^{4+} dissolved in conc. H_2SO_4 decreases by almost a factor of 3.

Formation of a solid solution was also concluded after comparing the thickness of the amorphous vanadia layer on VT_A-6 and VT_R-6 (Figs. 5 and 6), which is 2.5 and 1.5 nm, respectively. The comparison indicates that for VT_R-6, 40% of total vanadia could be in rutile. However, the chemical analysis of VT_R-6 shows 15% of V^{4+} and an additional 5% that is not dissolved in the treatments with NH_3(aq) and conc. H_2SO_4. A limit of 5% of the total vanadium in solid solution, which could be inferred from the missing part of vanadia in the chemical analysis, is not consistent with HREM images. To calculate the amount of vanadia from micrographs is difficult, which can at least explain the difference of a factor of two in the total amount of V^{4+} obtained from the two methods. Consequently, it seems that the titania interface is a solid solution of V^{4+} in rutile with a thickness of a few atomic layers. The fraction of monolayer vanadia given in Table 2 for rutile-supported catalysts can be obtained from the outer part of the titania interface, where the V^{4+} concentration is the highest. Possibly, parts of interconnected V^{+4} species in rutile are dissolved in the treatment with acid.

A clean, well-resolved axial resonance spectrum arising from a single type of isolated V^{4+} is observed for VT_R-1.9 in Fig. 3. Such spectral features, which have also been observed by others (*46*), are in agreement with the formation of a solid solution between vanadia and rutile. The separation distance and interaction with coordinated oxygen species reduce or eliminate V^{4+}–V^{4+} interaction. The VTM_R spectrum shows two overlapping features, one of which is virtually identifiable with that observed in VT_R-1.9. The second species shows the effect of dipolar broadening and may result from chemical changes in exposed vanadia, which are induced by the NH_3(aq)-washing process.

Superlayer region. On the three TiO_2 polymorphs, vanadium above the monolayer region according to chemical analysis is mainly V^{5+}, although ESR spectra show the presence of some V^{4+}. HREM images of VT_B-6, in the initial state, are without any

anomalous surface structure, e.g., Fig. 8a. This observation indicates the existence of epitaxially grown vanadia on TiO_2(B). The presence of vanadia at the catalyst surface is confirmed by the appearance of particles of reduced vanadium oxide, formed upon irradiation for a few minutes with a fully converged electron beam; cf. Fig. 8b. Additionally, small crystalline V_2O_5 particles are present as is shown in Fig. 9a. The formation of some crystalline V_2O_5 is also confirmed by the IR spectrum in Fig. 2.

On both anatase and rutile support, the formation of an amorphous overlayer of vanadium oxide is observed (Figs. 5 and 6). Considering the IR spectra in Fig. 2, it is clear that some crystalline V_2O_5 is present, especially on VT_A-6. The observation of formation of amorphous vanadia on anatase is consistent with earlier HREM work (*17, 47*). Unlike previous reports, neither an epitaxy between V_2O_5 and anatase (*47*), nor the formation of a thin rutile layer between the vanadia and anatase lattices (*47, 48*), could be observed using HREM. However, as was mentioned above, a small component of the ESR signal of the anatase-supported catalysts can be attributed to V^{4+} in a rutile-like environment.

Catalytic Performances

Consideration of Figs. 10–12 shows that for nitrile formation, the VTM_A and VTM_B monolayer catalysts are more active than those of higher loadings. However, for TiO_2(B)-supported samples, the selectivity for nitrile formation increases with increase in loading. Among the rutile-supported catalysts, VTM_R is less active but more selective than VT_R-6. Interestingly, all the true monolayer samples show poor performance for the oxidation of toluene to benzaldehyde. For this reaction, the catalysts with five theoretical vanadia layers are to be preferred, also when compared with crystalline V_2O_5.

The present finding that a monolayer on anatase (VTM_A) is good for toluene ammoxidation is in agreement with a study of the same reaction over vanadia/anatase catalysts prepared by flash-drying (*3*). In the latter investigation, contradictory to the present results, amorphous vanadia was concluded to be inactive. Concerning the oxidation to benzaldehyde, Table 3 shows VT_A-6 and VT_A-1.9 to be comparable. A catalytic performance, which is almost independent of the concentration of vanadia at intermediate loading, has also been observed using anatase and Degussa P25-supported catalysts for the oxidation of *o*-xylene to phthalic anhydride (*2, 8*) and toluene to benzoic acid (*7*). For these reactions, contradictory to the present results on aldehyde formation, it was concluded that monolayer species are both active and selective, while multilayers and V_2O_5 give a negligible contribution, due to either their small exterior surface or their low activity (*2, 7*).

With the increase in vanadia loading on rutile support, the catalytic performance in the oxidation of *o*-xylene has been reported to approach that of crystalline V_2O_5 (*8*). Another investigation (*9*) showed that the vanadia overlayer on rutile is unstable and shrinks to form a heterogeneous mixture of V_2O_5 and rutile. The present investigation, in agreement with an earlier report (*39*), shows the vanadia on rutile to be both structurally (Fig. 6) and catalytically (Figs. 10–12, Table 3) different from crystalline V_2O_5.

REFERENCES

1. Bond, G. C., and König, P., *J. Catal.* **77,** 309 (1982).
2. Wachs, I. E., Saleh, R. Y., Chan, S. S., and Chersich, C. C., *Appl. Catal.* **15,** 339 (1985).
3. Cavani, F., Foresti, E., Trifirò, F., and Busca, G., *J. Catal.* **106,** 251 (1987).
4. Cavalli, P., Cavani, F., Manenti, I., and Trifirò, F., *Catal. Today* **1,** 245 (1987).
5. Jonson, B., Rebenstorf, B., Larsson, R., and Andersson, S. L. T., *J. Chem. Soc. Faraday Trans. 1* **84,** 3547 (1988).
6. Sanati, M., and Andersson, A., *J. Mol. Catal.* **59,** 233 (1990).
7. van Hengstum, A. J., van Ommen, J. G., Bosch, H., and Gellings, P. J., *Appl. Catal.* **8,** 369 (1983).
8. Gasior, M., Gasior, I., and Grzybowska, B., *Appl. Catal.* **10,** 87 (1984).

9. Gasior, M., Haber, J., and Machej, T., *Appl. Catal.* **33,** 1 (1987).
10. Véjux, A., and Courtine, P., *J. Solid State Chem.* **23,** 93 (1978).
11. Kozłowski, R., Pettifer, R. F., and Thomas, J. M., *J. Phys. Chem.* **87,** 5176 (1983).
12. Bond, G. C., and Flamerz, S., *Appl. Catal.* **46,** 89 (1989).
13. Haber, J., Machej, T., and Czeppe, T., *Surf. Sci.* **151,** 301 (1985).
14. Cavani, F., Foresti, E., Parrinello, F., and Trifirò, F., *Appl. Catal.* **38,** 311 (1988).
15. Bond, G. C., Zurita, J. P., Flamerz, S., Gellings, P. J., Bosch, H., van Ommen, J. G., and Kip, B. J., *Appl. Catal.* **22,** 361 (1986).
16. Kijenski, J., Baiker, A., Glinski, M., Dollenmeier, P., and Wokaun, A., *J. Catal.* **101,** 1 (1986).
17. Baiker, A., Dollenmeier, P., Glinski, M., and Reller, A., *Appl. Catal.* **35,** 351 (1987).
18. Marchand, R., Brohan, L., and Tournoux, M., *Mater. Res. Bull.* **15,** 1129 (1980).
19. JCPDS International Centre for Diffraction Data, "Powder Diffraction File," Swarthmore, PA 1985.
20. Wallenberg, L. R., Sanati, M., and Andersson, A., *Microsc. Microanal. Microstruct.* **1,** 357 (1990).
21. Spurr, R. A., and Myers, H., *Anal. Chem.* **29,** 760 (1957).
22. Bachmann, H. G., Ahmed, F. R., and Barnes, W. H., *Z. Kristallogr.* **115,** 110 (1961).
23. Nakamura, M., Kawai, K., and Fujiwara, Y., *J. Catal.* **34,** 345 (1974).
24. Stadelmann, P. A., *Ultramicroscopy* **21,** 131 (1987).
25. Andersson, A., and Hansen, S., *J. Catal.* **114,** 332 (1988).
26. Busca, G., Marchetti, L., Centi, G., and Trifirò, F., *J. Chem. Soc. Faraday Trans. 1* **81,** 1003 (1985).
27. Feil, F. S., van Ommen, J. G., and Ross, J. R. H., *Langmuir* **3,** 668 (1987).
28. Busca, G., and Lavalley, J. C., *Spectrochim. Acta, Part A* **42,** 443 (1986).
29. Busca, G., Centi, C., Marchetti, L., and Trifirò, F., *Langmuir* **2,** 568 (1986).
30. Abello, L., Husson, E., Repelin, Y., and Lucazeau, G., *Spectrochem. Acta, Part A* **39,** 641 (1983).
31. Liu, Z., Lin, Z., Fan, H., Li, F., Bao, Q., and Zhang, S., *Appl. Phys. A* **45,** 159 (1988).
32. Smith, D. J., McCartney, M. R., and Bursill, L., *Ultramicroscopy* **23,** 299 (1987).
33. Wallenberg, L. R., Sanati, M., and Andersson, A., *J. Catal.* **126,** 246 (1990).
34. Véjux, A., and Courtine, P., *J. Solid State Chem.* **63,** 179 (1986).
35. Andersson, B., Gjönnes, J., and Taftö, J., *Acta Crystallogr. Sect. A* **30,** 216 (1974).
36. Wallenberg, L. R., Andersson, A., and Sanati, M., *Ultramicroscopy* **34,** 33 (1990).
37. Théobald, F., Cabala, R., and Bernard, J., *J. Solid State Chem.* **17,** 431 (1976).
38. Yoshida, S., Iguchi, T., Ishida, S., and Tarama, K., *Bull. Chem. Soc. Jpn.* **45,** 376 (1972).
39. Cavani, F., Centi, G., Foresti, E., Trifirò, F., and Busca, G., *J. Chem. Soc. Faraday Trans. 1* **84,** 237 (1988).
40. Jansen, S., Tu, Y., Palmieri, M. J., Sanati, M., and Andersson, A., submitted for publication.
41. Haber, J., Kozłowska, A., and Kozłowski, R., *J. Catal.* **102,** 52 (1986).
42. Roozeboom, F., Fransen, T., Mars, P., and Gellings, P. J., *Z. Anorg. Allg. Chem.* **449,** 25 (1979).
43. Cavani, F., Centi, G., Parrinello, F., and Trifirò, F., *in* "Preparation of Catalysts IV" (B. Delmon, P. Grange, P. A. Jacobs, and G. Poncelet, Eds.), Studies in Surface Science and Catalysis, Vol. 31, p. 227. Elsevier, Amsterdam, 1987.
44. Cristiani, C., Forzatti, P., and Busca, G., *J. Catal.* **116,** 586 (1989).
45. Andersson, A., and Andersson, S. L. T., *in* "Solid State Chemistry in Catalysis" (R. K. Grasselli and J. F. Brazdil, Eds.), ACS Symposium Series, Vol. 279, p. 121. American Chemical Society, Washington, DC, 1985.
46. Rusiecka, M., Grzybowska, B., and Gasior, M., *Appl. Catal.* **10,** 101 (1984).
47. Kang, Z. C., and Bao, Q. X., *Appl. Catal.* **26,** 251 (1986).
48. Machej, T., Ruiz, P., and Delmon, B., *J. Chem. Soc. Faraday Trans.* **86,** 731 (1990).